Development of a Family of Redox-Sensitive Green Fluorescent Protein Indicators for Use in Relatively Oxidizing Subcellular Environments[†,‡]

Jeremy R. Lohman[§,||] and S. James Remington*[,§,⊥]

Institute of Molecular Biology and Departments of Chemistry and Physics, University of Oregon, Eugene, Oregon 97403

Received March 23, 2008; Revised Manuscript Received June 20, 2008

ABSTRACT: Green fluorescent protein (GFP) indicators were previously developed that rapidly and quantitatively respond to changes in the thiol/disulfide equilibrium within subcellular compartments. In these indicators, surface-exposed cysteines residues were introduced so as to form a labile redox-active disulfide that in turn controls the emission properties of the internal chromophore. The biosensors have been shown to be effective reporters of the thiol/disulfide status within reducing compartments such as the mitochondria and cytosol for several cell types. However, due to the high thermodynamic stability of the introduced disulfide bond, the indicators are not useful for quantitative analysis within more oxidizing compartments such as the endoplasmic reticulum. Here we report the development of a new family of GFP-based redox indicators (roGFP1-iX) in which the thermodynamic stability of the disulfide is substantially lowered by insertion of a single amino acid into the main chain, adjacent to cysteine 147. The insertions result in indicators with midpoint potentials of −229 to −246 mV and are thus better suited for study of relatively oxidizing subcellular compartments. Atomic resolution crystallographic analyses suggest that two important factors act to destabilize the disulfide linkage in roGFP1-iX. In the oxidized state, an unusual non-proline cis-peptide bond adjacent to one of the cysteines introduces geometric strain into the system, while in the reduced state, a dramatic loop opening lowers the effective concentration of the reacting species.

Redox-sensitive green fluorescent proteins (roGFP) have previously been developed and shown to be effective indicators of cellular thiol/disulfide equilibrium; however, quantitative readout is limited to a range defined by the thermodynamic midpoint potential of the reactive components. The indicators were produced by substitution of cysteine residues on the surface of GFP,[1] which can form a disulfide bond without substantially distorting the structure of the protein. On a background of wild-type or GFP-S65T, Hanson et al. substituted cysteines residues at positions Ser147 and Gln204 (to create roGFP1 and roGFP2, respectively) or Asn149 and Ser202 (to create roGFP3 and roGFP4, respectively) (*1*). Using the same approach but on the background of the yellow fluorescent variant YFP (λ^{em}_{max} = 525 nm), Ostergaard et al. produced rxYFP$^{N}_{C}$, where N and C are integers indicating the locations of the introduced cysteines (*2*).

In vitro and in vivo, these two families of indicators show two-state changes in fluorescence emission in response to the ambient thiol/disulfide ratio. roGFP indicators are ratiometric by excitation, that is, they exhibit two excitation peaks (at about 390 and 475 nm), corresponding to the neutral and anionic chromophore forms, respectively. Excitation of either peak gives rise to green fluorescence at about 510 nm. Upon oxidation of the redox-sensitive disulfide, the population of the neutral chromophore is favored at the expense of the anionic chromophore; however, an isosbestic point at 425 nm exists because the emission intensities from the neutral and the anionic chromophore are identical when excited at this wavelength. This feature allows one to deduce the roGFP indicator concentration, independent of the oxidation state. In contrast, rxYFPs have a single fluorescence excitation peak (at ∼512 nm) which varies in amplitude depending on the oxidation state; thus these indicators are not ratiometric. Ratiometric behavior allows one to correct for a number of factors influencing the fluorescence intensity such as cell thickness, protein expression level, and photobleaching. Single peak reporter use is, in practice, limited to bulk cell suspensions in solution (*3*). However, most other properties of the two families of indicators are very similar.

As determined by simple titrations against thiol/disulfide redox buffers such as DTT or lipoic acid, the midpoint potentials of roGFP1, roGFP2, and rxYFP$^{149}_{202}$ have been reported to be −287 mV (*1*), −272 mV (*1*), and −261 mV (*2*), respectively. Compared to the midpoint potential of the

[†] This work was supported by grants from the National Institutes of Health (5R01GM042618-16 to S.J.R.) and American Heart Association (predoctoral fellowship to J.R.L.).

[‡] The atomic coordinates and structure factors have been deposited in the Protein Data Bank (entries 3CB9 for roGFP1-iR oxidized, 3CBE for roGFP1-iR reduced, 3CD1 for roGFP1-iE oxidized, and 3CD9 for roGFP1-iE reduced).

* To whom correspondence and reprint requests should be addressed. Tel: (541) 346-5190. Fax: (541) 346-5870. E-mail: jremington@uoxray.uoregon.edu.

[§] Institute of Molecular Biology, University of Oregon.

[||] Department of Chemistry, University of Oregon.

[⊥] Department of Physics, University of Oregon.

[1] Abbreviations: GFP, green fluorescent protein; YFP, yellow fluorescent protein; DTT, dithiothreitol; GSSG, glutathione oxidized; GSH, glutathione reduced; TCEP, tris(2-carboxyethyl)phosphine; NADPH, reduced nicotinamide adenine dinucleotide phosphate.

10.1021/bi800498g CCC: $40.75
Published on Web 07/25/2008

GSSG-GSH couple (−240 mV (*4*)), these indicators are considered reducing and are thus best suited for use in reducing subcellular environments such as mitochondria or the cytoplasm. roGFPs have been used to determine the thiol/disulfide equilibrium within the mitochondria ($E_{pH=8} \sim -360$ mV) (*1*) and cytoplasm ($E_{pH=7} \sim -320$ mV) (*5*) of single HeLa cells, as well in *Arabidopsis* (mitochondria $E_{pH=7.8} = -362 \pm 10$ mV and cytoplasm $E_{pH=7} = -318 \pm 13$ mV (*6*)). The cytosolic thiol/disulfide equilibrium of *Saccharomyces cerevisiae* and *Escherichia coli* has been determined using rxYFP$^{149}_{202}$ to be −289 and −259 mV, respectively (*2, 7*). However, in all of these probes, the reactive disulfide bond is too stable to permit quantitative readout of the redox potential in more oxidizing environments such as the endoplasmic reticulum (estimated reduction potential -180 ± 6 mV (*8*)); that is, in such an environment, the probes are completely oxidized (*7, 9, 10*). For example, Austin et al. (*10*) used roGFP1 to suggest that, contrary to the prevailing misconception, the environment within the endocytotic pathway in human prostate cancer PC3 cells is oxidizing rather than reducing. However, within that context the probe was oxidized to saturation so a quantitative result could not be reported.

Thus, there is a clear need to extend the range of midpoint potentials over which redox-sensitive GFPs can be used as quantitative reporters. One attractive approach to extend this range is to reengineer existing GFP-based indicators to lower the thermodynamic stability of the reactive disulfide. In nature, midpoint potentials of protein disulfides cover an extremely large range that spans the relevant physiological states. Considering only those proteins that are catalytically active in establishing thiol/disulfide equilibrium processes, the midpoint potentials of the thiol/disulfide oxidoreductases range from −270 mV for *E. coli* thioredoxin (*11*) to −122 mV for DsbA (*12*). This range of midpoint potentials corresponds to a range of approximately 5 orders of magnitude in the equilibrium constants for disulfide formation.

From studies of thiol/disulfide oxidoreductases (*13*), peptides, and small dithiol-containing molecules (*14, 15*), it is clear that several factors affect the thermodynamic stability of disulfides. These factors include thiol pK_a, geometric strain, and entropic effects. Approaches to modify disulfide stability could in principle make effective use of any one or a combination of these factors. One approach is to decrease the pK_a of one or both of the participating thiols, stabilizing the reactive thiolate species (*16*). In practice, this has been achieved by substitution of one or more positively charged residues close to the reactive disulfide. The success of such approaches has been discussed in detail for roGFP1 (*17*) and rxYFP$^{149}_{202}$ (*18*). For example, in roGFP1, substitution of three arginine or lysine residues near the disulfide increased the midpoint potential by 16 mV. In addition, the substitutions had the effect of increasing the rates of oxidation and reduction, for a 4.9-fold increase in oxidation rate constant by H_2O_2 and 6.0-fold increase in the DTT reduction rate constant (*17*). Similarly, placement of three arginine residues near the disulfide of rxYFP$^{149}_{202}$ led to a 4.3-fold increase in the rate of oxidation by oxidized β-mercaptoethanol and 13-fold increase in the rate of oxidation by GSSG (*18*). In the latter, the changes in indicator midpoint potentials were not reported, and part of the observed rate increase can be attributed to electrostatic effects on substrate diffusion.

Two other approaches, which are often linked, are to introduce geometric strain into the disulfide linkage or to change entropic factors associated with the reaction. For example, with small molecules that undergo ring closure upon disulfide formation, decreasing the ring size below six atoms increases the midpoint potential because the disulfide cannot achieve the lowest energy geometry, whereas increasing the ring size above six increases the entropic barrier to disulfide formation. The latter effect may also be thought of as lowering the effective concentration of the reacting thiols (*19, 20*). There is a similar relationship for peptides containing cysteine residues. Cysteines that are immediately adjacent to each other or separated by one intervening residue do not readily form disulfides, which is thought to be due to geometric strain, but beyond a certain size, increasing the length of the peptide decreases disulfide stability due to entropic effects (*16, 21–23*).

In proteins, the addition or deletion of residues flanking the disulfide may additionally increase or decrease disulfide stability, depending upon how the protein rearranges to accommodate the insertion or deletion. In one example, the deletion of the proline from the active site peptide -CPGC- to produce -CGC- in thioredoxin destabilized the disulfide bond (toward a more oxidizing midpoint potential) to ≥ −200 mV compared to −270 mV for wild-type (*24*).

Here we describe efforts to use single amino acid insertions to destabilize the redox-sensitive disulfide bridge of a redox-sensitive GFP, in order to produce a roGFP suitable for relatively oxidizing subcellular environments. An additional requirement was that the roGFP exhibit ratiometric response to changes in the ambient thiol/disulfide equilibrium. Equilibrium and kinetic measurements indicate that, for one class of insertion mutants (roGFP1-iX), the disulfide is substantially destabilized, showing higher rates of reduction and lower rates of oxidation compared to the parent molecule roGFP1. Crystal structure analysis of two variants in the oxidized and reduced states verified disulfide formation in the oxidized state and revealed large conformational changes associated with oxidation/reduction. The factors contributing to disulfide stability are discussed in the light of the atomic models.

MATERIALS AND METHODS

Experimental Approach and Mutational Analysis. Initially, we chose to insert a single glycine residue on either side of the cysteine residues (147 and 204) participating in the redox-sensitive disulfide of roGFP1 and roGFP2. Glycine has the fewest restrictions on backbone conformation, and thus in principle the insertion could be accommodated by the protein in a variety of ways. Glycine-containing mutants, four each for roGFP1 and roGFP2, were produced and purified; those that were shown to have spectra sensitive to addition of reductants were characterized further by titration against DTT and lipoic acid. Of those characterized, none exhibited a response that was ratiometric by excitation. Instead, these mutants exhibited a general increase in fluorescence upon reduction of the presumed disulfide linkage, similar to the behavior of rxYFP (*18*). However, one variant, roGFP2 containing a glycine insertion between Cys147 and His148 (roGFP2-C147CG), was found by titration to have a thermodynamically destabilized disulfide. This variant was then

subjected to random and directed mutagenesis with two objectives in mind. The first objective was to produce a variant with ratiometric response to changes in the ambient thiol/disulfide equilibrium, while the second objective was to investigate the consequences of side chain size and charge at the insertion position on the thermodynamic stability of the disulfide linkage.

It has long been known that wild-type GFP does not fold efficiently at 37 °C (*25*); therefore, to improve the screening process, the so-called "folding mutations" (F64L, F99S, M153T, V163A, and I167T; see refs *25–27*) were incorporated into roGFP2-C147CG. The same mutations were introduced into roGFP1 (roGFP1-C147CG). Residues near the putative disulfide and known to influence the protonation state of the chromophore (Gly147a, His148, Thr203, and Ser205) were chosen for randomization in that background. Visibly fluorescent bacterial colonies were picked, the GFP gene was sequenced, and protein was expressed in small quantities overnight, purified, and finally subjected to SDS−PAGE analysis to assess aggregation under oxidizing conditions. Those variants that formed dimers or higher aggregation states were rejected. Variants that survived this selection were further characterized by fluorescence spectroscopy.

Gene Construction, Mutagenesis, and Protein Expression/Purification. roGFP1 (GFP with C48S/S147C/Q204C) in $pRSET_B$ was PCR amplified using primers containing *Bam*HI and *Hind*III cut sites and cloned into the pQE-30 expression vector containing an N-terminal His_6 tag. To produce the initial insertions and all other nonrandom mutations, the QuikChange (Stratagene) protocol was utilized.

Random mutations were introduced at four codons using the Stratagene multi-site-directed mutagenesis kit, and the plasmids were transformed into DH5α cells. Two primers were utilized, one randomizing positions Gly147a and His148 simultaneously and the other randomizing positions Thr203 and Ser205. Visibly fluorescent colonies were picked and used to inoculate 2 mL of growth media for overnight culture. DNA sequencing of the GFP coding region was used to identify all mutations.

roGFP1 and the initial insertion mutants were prepared from $pRSET_B$ plasmids as described previously (*1, 17*). Random insertion mutants in plasmid pQE-30 were expressed in *E. coli* strain DH5α by allowing cultures to reach an OD_{600} of between 0.4 and 0.9 at 37 °C, at which point the temperature was reduced to 25 °C overnight. No IPTG was required for efficient protein production. Cells were pelleted by centrifugation and resuspended in 50 mM HEPES (pH 7.9), 300 mM NaCl, and 10% glycerol. The cells were frozen, thawed, and then sonicated for 5 min. Cell lysate was centrifuged, and the supernatant was applied to a column of Ni^{2+}-agarose resin (Qiagen) for purification. Samples were dialyzed into 20 mM Tris (pH 8.0) and 1 mM EDTA and further purified using anion exchange. Pure fractions were concentrated by filtration and buffer exchanged into 20 mM HEPES (pH 7.9).

Spectroscopy. Fluorescence excitation/emission scans and kinetic traces were determined using a LS55 fluorescence spectrophotometer (Perkin Elmer Life Sciences) or a FluoroMax-3 fluorescence spectrophotometer (Jobin Yvon Inc.). Fluorescence quantum yields were determined using protein samples that had A_{400} equal to a 9-aminoacridine standard. Emission spectra were corrected for photomultiplier wavelength sensitivity and integrated as described previously (*17, 28*). Wild-type GFP and roGFP1 were utilized as controls.

Midpoint Potential Determinations. To minimize O_2-mediated oxidation, all solutions and samples were prepared/incubated in a glovebox. Protein samples were prepared at ~1 μM in 100 mM HEPES (pH 7.0), 300 mM NaCl, and 1 mM EDTA with 2.5 mM total lipoic acid (mixture of oxidized and reduced forms) and allowed to equilibrate for 3−4 h. After equilibration, samples were removed and fluorescent spectra were determined at 25 °C. Apparent redox midpoint potentials for the mutants were determined by the method of Hanson et al. (*1*). To determine the fraction reduced *R* of the roGFP indicator, intensity ratios of 505 nm fluorescence for excitation at the isosbestic point (425 nm) and at 465 nm were used in the analysis as follows.

F denotes the ratio between 505 nm fluorescence intensity values of a sample excited at two wavelengths (e.g., at 465 nm over 425 nm). F_{red} and F_{ox} represent ratios of fluorescence intensities of fully reduced and fully oxidized samples of the indicator protein, respectively. The raw measures of fluorescence intensity, *I*, should be background corrected if possible. For example

$$F_{red} = I_{red,465}/I_{red,425} \quad (1)$$

R denotes the fraction of the roGFP indicator that is in the reduced form in the sample, which is

$$R = (F - F_{ox})/(F_{red} - F_{ox}) \quad (2)$$

The ratio of the reduced over oxidized roGFP indicator is conveniently calculated as

$$R/(1 - R) = (F - F_{ox})/(F_{red} - F) \quad (3)$$

Equation (3) is valid only if the denominator wavelength is the isosbestic point (425 nm). For the more general case of two arbitrarily chosen wavelengths, a correction factor must be applied. Following the analysis given in ref *3*, one obtains

$$\frac{R}{1-R} = \frac{F - F_{ox}}{F_{red} - F}\left(\frac{I_{ox,\lambda 2}}{I_{red,\lambda 2}}\right) \quad (4)$$

where the values of *F* can now be defined more freely as ratios of fluorescence intensities at two arbitrary wavelengths, λ_1 and λ_2, as follows:

$$F = I_{\lambda 1}/I_{\lambda 2}$$

$$F_{ox} = I_{ox,\lambda 1}/I_{ox,\lambda 2}$$

$$F_{red} = I_{red,\lambda 1}/I_{red,\lambda 2}$$

The midpoint potential ($E^{\circ\prime}$) of the roGFP under investigation was determined by titration against lipoic acid, with $E^{\circ\prime}$ assumed to be −0.290 V (*15*). All titrations were performed at least twice. When roGFPs are used as indicators in vivo, the ambient reduction potential can be deduced by using the Nernst equation, where the *RT*/*nF* term has been evaluated at 298 K

$$E^{\circ\prime}_{ambient} = E^{\circ\prime}_{roGFP} - 29.6\ mV \log(R/(1 - R)) \quad (5)$$

Oxidation/Reduction Kinetics. Reaction rates for reduction of redox-sensitive GFPs by DTT and oxidation by oxidized cysteine (cystine or CSSC) were determined by addition of

Table 1: roGFP-iX Redox Potential and Kinetic and Spectroscopic Properties

Xins[a]	$E^{o\prime}$ [b]	reduction rate[c]	oxidation rate[d]	Φ[e]	δ[f]	λ_{em} 400nm ex	λ_{iso} 505nm em
L	-229 ± 5	0.77	0.22	0.30	7.2	505	425
E	-236 ± 7	0.33	0.14	0.31	4.5	503	425
Q	-239 ± 6	0.33	0.21	0.31	4.1	505	425
H	-238 ± 4	0.47	0.22	0.33	3.1	505	425
R	-237 ± 5	0.27	0.22	0.24	2.9	502	425
S	-240 ± 3	0.48	0.24	0.31	2.4	505	425
D	-246 ± 1	0.23	0.18	0.24	2.8	502	425
roGFP1	-287	0.18	0.33	0.64	6.5	508	425

[a] Mutations roGFP1 (C48S/S147C/Q204C) + X insertion/H148S/F64L/F99S/M153T/V163A/I167T. [b] Titration against 2.5 mM lipoic acid. [c] Reduction by 1 mM DTT in units of min^{-1}, standard deviation less than ± 0.05 (at least two trials). [d] Oxidation by 1 mM cystine in units of min^{-1}, standard deviation less than ± 0.05 (at least two trials). [e] Fluorescence quantum yield from excitation at 400 nm. [f] Dynamic range is the maximum observed δ-fold change in excitation peak ratio.

a large excess of reagent (1 mM) and monitoring fluorescence over time. Solutions were degassed prior to use, and experiments were conducted at 25 °C, with ~1 μM protein in 100 mM HEPES (pH 7.0), 300 mM NaCl, and 1 mM EDTA. Prior to oxidation by CSSC, concentrated protein samples (~50 μM) were incubated with ~1 mM DTT for 1 h to reduce the protein. The remaining DTT was removed by using gel filtration spin columns. Pseudo-first-order rate constants were determined from the fluorescence emission data by fitting the reaction progress curves to single-exponential functions using KaleidaGraph (Synergy Software).

Crystal Structure Determination. roGFP1-iR protein (oxidized; see Table 1 for nomenclature) was concentrated to ~25 mg/mL in 20 mM HEPES, pH 7.9. Crystals grew in 1−2 days by hanging drop vapor diffusion against 0.1 M Tris (pH 8.5), 22−24% PEG 1550, and 0−0.06 M $MgCl_2$. Drops consisted of 1 μL of protein and 1 μL of well solution. Crystals of oxidized roGFP1-iR were transferred to a sitting drop (initially 10 μL of mother liquor), and artificial mother liquor containing 0.1 M Tris, pH 8.0, 30% PEG 1550, 0.05 M $MgCl_2$, and 20 mM TCEP was added gradually over the course of 2 days (final drop volume was 50 μL) to obtain crystals with reduced cysteines.

roGFP1-iE protein (oxidized; see Table 1 for nomenclature) was concentrated to ~25 mg/mL in 20 mM HEPES (pH 7.9). Crystals grew in ~7 days by hanging drop vapor diffusion against 0.1 M Tris (pH 8.0), 24% PEG 1550, and 0.04 M sodium acetate. Again, TCEP (20 mM) was used to reduce crystals except the final condition was 0.1 M Tris (pH 8.0), 30% PEG 1550, and 0.05 M sodium acetate.

X-ray diffraction data were collected from single frozen crystals for both mutants in both the oxidized and the reduced state at the Advanced Light Source (ALS) beamline 5.0.1. Data sets were indexed and reduced using the HKL2000 suite (*29*). Molecular replacement solutions were found with Molrep using the GFP-S65T coordinate file (PDB code 1EMA) as the search model. ARP/wARP was used to rebuild the model (*30*). Refmac 5 (*31*) was used for further refinement after model building in Coot (*32*). Water molecules placed by ARP/wARP were retained only if they were associated with reasonable electron density peaks and had appropriate proximity to hydrogen-bonding partners.

RESULTS

Expression of roGFP1 and roGFP2 plasmids containing single glycine insertions adjacent to Cys204 resulted in soluble but nonfluorescent protein of the appropriate molecular weight. This material was not further characterized. However, single glycine insertions adjacent to Cys147 yielded fluorescent protein. Partial purification and characterization of roGFP2-S147GC (with a glycine inserted N-terminal to the cysteine) suggested that this molecule was responsive to changes in the ambient thiol disulfide equilibrium in vitro. However, the estimated midpoint potential (~−285 mV) was close to that of the original roGFP2, and hence this variant was not further characterized. Promising behavior resulted from insertion of a glycine C-terminal to Cys147 (roGFP2-S147CG). Preliminary tests suggested that a disulfide formed under oxidizing conditions, yet had significantly decreased thermodynamic stability (~−255 mV) compared to roGFP2. Oxidized roGFP2-S147CG (emission at ~508 nm) has a single excitation peak at 490 nm, which increases in amplitude upon reduction with lipoic acid. Random mutagenesis at positions 147a and 148 was successfully applied to recover ratiometric behavior of fluorescence excitation upon oxidation/reduction. The resulting mutations were highly variable at position 147a but, more importantly, incorporated serine instead of histidine at position 148 (see Table 1).

In this way, a promising family of variants was obtained (roGFP1−147CX/H148S, containing additional folding mutations; see Table 1). Several members of the family were characterized in some detail. To identify members of this family, we have adopted the shorthand notation roGFP1-iX, where X denotes the amino acid at insertion position 147a.

Spectroscopic Properties of roGFP1-iX. The characterized members of the roGFP1-iX family have excitation and emission spectra similar to the roGFP series, with excitation peaking at ~395 nm (band A) and ~465 nm (band B), while fluorescence emission peaks at ~505 nm. The relative amplitudes of the excitation peaks depend strongly on the presumed oxidation state of the 147−202 disulfide. In the oxidized state, excitation band A is favored over the band B; however, upon reduction, band B becomes dominant (Figure 1). The behavior is two-state with an isosbestic point at ~425 nm. Fluorescence quantum yields for excitation at 400 nm are somewhat lower than wild-type GFP or roGFP1 and range from about 0.24 (roGFP1-iD) to 0.33 (roGFP1-iH). Table 1 summarizes the spectral and biochemical properties of the variants. The dynamic range δ (defined as the maximum observed ratio of excitation peak ratios) spans from 2.4 (roGFP1-iS) to 7.2 (roGFP1-iL) and is comparable to that of roGFP1 (6.5) (*1*).

While the excitation spectrum of wild-type GFP is insensitive to solution pH over the range of about 4−10 (*25, 33, 34*), most mutations close in space to and including His148 confer pH sensitivity, and roGFP1-iX mutants are no exception. The excitation spectra of oxidized roGFP1-iE is quenched at low pH, and compared to behavior at pH 7.0 the fluorescence intensity is reduced by a factor of 2 at pH 6.0 (see Figure S1 in Supporting Information). As the pH is increased above 8.0, the fluorescence excitation spectrum shows a reduction in the amplitude of the 395 nm peak in

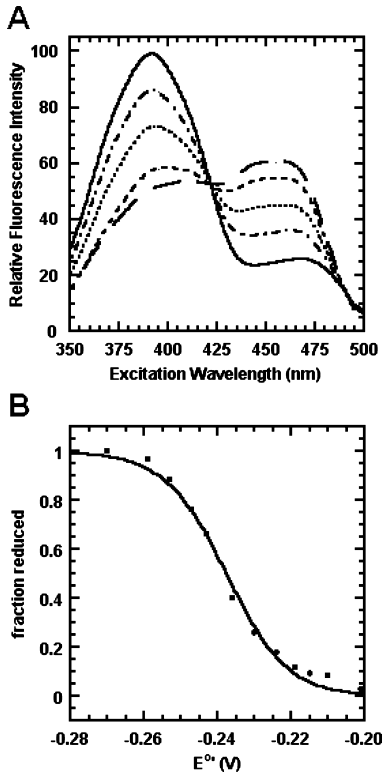

FIGURE 1: Redox titration of roGFP1-iE. (A) Fluorescence excitation spectra, monitoring emission at 505 nm, at the following redox potential values: −181 (solid line), −224 (dashed and dotted line), −236 (dotted line), −247 (short dashed line), and −390 mV (long dashed line). (B) Fraction reduced, determined from excitation ratios, as a function of ambient potential. The solid line is the theoretical curve for a two-state transition with midpoint potential −236 mV.

favor of the 465 nm peak. Reduced roGFP1-iE behaves similarly. Compared to pH 7.0, fluorescence intensity is reduced by a factor of 2 at pH 5.5, and above pH 9.5, the 465 nm peak becomes favored. The 465/395 ratio is essentially constant for both oxidized and reduced spectra between pH 6.0 and 8.0, suggesting that pH artifacts in this range are negligible (see Figure S2 in Supporting Information). The spectral pH dependence of roGFP1-iL and roGFP1-iR is similar to that of roGFPiE (data not shown).

Redox Equilibrium and Reaction Kinetics. Redox midpoint potentials were determined from the equilibrium constant of the reaction between roGFP1-iX and lipoic acid ($E^{\circ\prime}$ assumed to be −290 mV (*15*)). Redox midpoint potentials ranging from −229 mV (roGFP1-iL) to −246 mV (roGFP1-iD) are summarized in Table 1.

Pseudo-first-order rate constants for the reduction of the variants range from k_{DTT} 0.23 min^{-1} (roGFP1-iD) to k_{DTT} 0.77 min^{-1} (roGFP1-iL); see Table 2. The estimated error is less than ±0.05 as determined from at least two measurements. The oxidation rates were determined under similar conditions using 1 mM cystine (CSSC). Rate constants for the oxidation reactions varied from k_{CSSC} 0.14 min^{-1} (roGFP1-iE) to k_{CSSC} 0.24 min^{-1} (roGFP1-iS). Reversibility was verified by comparison of spectra obtained before and after oxidation/reduction kinetic trials, normalized to the isosbestic point to account for small changes in indicator concentration. By comparison, roGFP1 is reduced more slowly (k_{DTT} 0.18 min^{-1}, close to previously reported value of 0.13 min^{-1} (*17*)) than any of the roGFP1-iX, yet it is oxidized more rapidly (k_{CSSC} 0.33 min^{-1}).

Crystal Structure Analyses. roGFP1-iR and roGFP1-iE crystallized in space group $P2_12_12_1$, approximately isomorphous to crystals described for GFP-S65T (ref *35*, PDB ID code 1EMA). There is one molecule per asymmetric unit. Data collection to atomic resolution and refinement statistics can be found in Table 2 for all atomic models described below. As expected, each model is very similar to that of wild-type or GFP-S65T and consists of an 11-stranded β-barrel with an internal helix from which the chromophore forms (for structural overview see Figure 3). However, as detailed below, there are significant differences localized to the site of the amino acid insertion (position 147a) that are strongly influenced by the state of oxidation of the 147−204 disulfide.

Oxidized roGFP1-iR. Crystals of the oxidized form of roGFP1-iR diffracted to better than 1.31 Å resolution at ALS beamline 5.0.1, with the data resolution being limited by detector geometry. The final model consists of residues 3−231 with none in the disallowed regions of the Ramachandran diagram. The final model has an *R*-factor of 0.152 and an *R*-free of 0.169 at 1.31 Å resolution. Residues Asn146, Cys147, Arg147a, Ser148, and Cys204 are all clearly defined by the electron density maps. For representative electron density see Figure 4. Residues Cys147 and Cys204 form a disulfide that spans two adjacent segments of β-sheet and is in the pg^-t conformation (positive χ_{ss} torsion angle with a "gauche$^-$" χ^{1n} value of about −60° and "trans" χ^{1c} value of ± 180° (*36*)); see Table 3. For comparison, the torsion angles describing the disulfides found in other redox-sensitive GFPs are included in Table 3. As described in the study of disulfide conformations by Srinivasan et al. (*36*), there are relatively few disulfides in this conformation (2 of the 72 studied); the closest examples are found in immunoglobulin Fab (PDB ID code 1FB4, H chain residues Cys101 and Cys104) and in human lysozyme (PDB ID code 1LZ1, residues Cys77 and Cys95).

Remarkably, the peptide bond between Cys147 and Arg147a is in the rare cis conformation (*37*). The side chain of Arg147a spans the gap between the strands containing the disulfide and forms hydrogen bonds with Ser202 and the backbone carbonyl of Phe223. In addition, the hydrophobic side chain of the arginine is adjacent to the disulfide linkage, partially shielding it from solvent. The hydroxyl of Ser148 (which replaces His148 found in wild type GFP) forms a hydrogen bond to the chromophore hydroxyl group. The chromophore itself is slightly distorted from the cis-coplanar configuration, with twist and tilt angles of 1.3 and 9.6°, respectively (*38, 39*), which may explain the somewhat lowered fluorescence efficiency.

Reduced roGFP1-iR. Reduced roGFP1-iR crystals diffracted well, and data collection statistics were acceptable for data collected to 1.49 Å resolution. The final model consists of residues 2−231 with none in the disallowed regions of the Ramachandran plot. The final crystallographic *R*-factor is 0.165 and *R*-free is 0.188. The polypeptide backbone for residues Asn146, Cys147, Arg147a, and Ser148 is clearly defined in the density map, and while the side chains are found in slightly weaker density, a satisfactory model could be constructed. A large conformational change is observed for residues 146−147a relative to the oxidized

Table 2: Data Collection and Refinement Statistics

data collection	iE oxidized	iE reduced	iR oxidized	iR reduced
crystal				
total observations	180776	125308	190447	136444
unique reflections	52564	35231	54553	41093
cell dimensions (*a*, *b*, *c*) (Å)	51.2, 62.4, 68.8	51.2, 62.3, 69.6	51.1, 62.7, 70.1	51.0, 62.4, 68.8
resolution (Å)	50.0−1.31	50.0−1.50	50.0−1.31	50.0−1.40
highest resolution shell (Å)	1.36−1.31	1.55−1.50	1.36−1.31	1.45−1.40
completeness[a] (%)	98.6 (92.4)	97.2 (95.1)	99.5 (99.8)	93.3 (93.6)
averageI/s[a]	20.4 (1.9)	28.1 (2.1)	29.8 (9.8)	20.0 (1.6)
R_{merge}[a,b]	0.051 (0.429)	0.040 (0.472)	0.039 (0.098)	0.044 (0.449)
refinement				
space group	$P2_12_12_1$	$P2_12_12_1$	$P2_12_12_1$	$P2_12_12_1$
no. of molecules[c]	1	1	1	1
no. of protein atoms[c]	1834	1809	1843	1837
no. of solvent atoms[c]	263	244	303	239
resolution range (Å)	30.0−1.31	30.0−1.50	30.0−1.31	30.0−1.49
crystallographic *R*-factor[d]	0.164	0.167	0.152	0.165
R-free	0.184	0.193	0.169	0.188
average *B*-factors (Å^2)				
protein atoms	13.9	18.1	9.7	13.5
solvent	25.2	29.1	20.2	23.9
rmsd from ideality				
bond lengths (Å)	0.007	0.010	0.007	0.010
bond angles (deg)	1.404	1.469	1.367	1.478

[a] Values in parentheses indicate statistics for the highest resolution shell. [b] $R_{merge} = \sum|I - \langle I\rangle|/\sum\langle I\rangle$, where I is the observed intensity and $\langle I\rangle$ is the average of intensities obtained from multiple observations of symmetry-related reflections. [c] Per asymmetric unit. [d] *R*-factor $= \sum||F_o| - |F_c||/\sum|F_o|$, where F_o and F_c are the observed and calculated structure amplitudes, respectively.

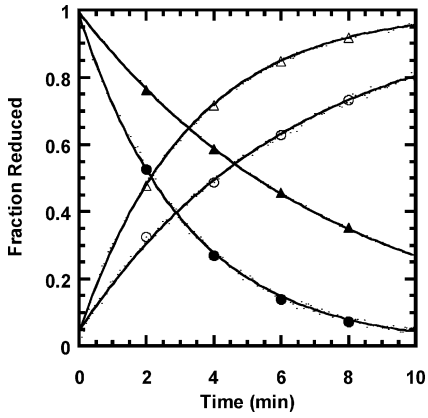

FIGURE 2: Oxidation and reduction progress curves for roGFP1 (circles) and roGFP1-iE (triangles). The fraction reduced over time is shown after addition of DTT (open markers) or oxidized cysteine (filled markers). Pseudo-first-order rate constants were determined by fitting the rate curves (solid lines) to a single exponential.

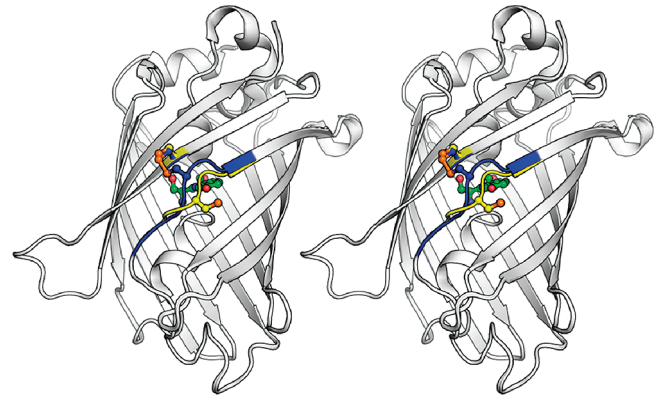

FIGURE 3: Stereo image structural overview of roGFP1-iR in oxidized and reduced states. The structures are identical except for the region of the insertion, shown in blue for the oxidized form and in yellow for the reduced form (cysteines in ball-and-stick representation). The centrally located chromophore is shown in green ball-and-stick representation.

state and the peptide bond between residues 147 and 147a is in the normal trans configuration (see later section for a more detailed comparison). The side chains for both Cys147 and Cys204 are statistically disordered and were modeled in two conformations. Ser148 is hydrogen bonded to the chromophore, whereas Arg147a forms a salt bridge with Asp117 of a symmetry-related molecule. The chromophore twist and tilt angles are 0.7 and 11° respectively (*38*).

roGFP1-iE. Diffraction data for oxidized roGFP1-iE were collected to 1.31 Å resolution and show good statistics. The final model consists of residues 3−147 and 148−231 with none in the disallowed regions of the Ramachandran plot. The final crystallographic *R*-factor is 0.164 and *R*-free is 0.184. Electron density is clear for all groups adjacent to the disulfide except for the inserted amino acid Glu147a. Although weak density is present for the main chain at position 147a, it was not considered sufficient to permit modeling of a single conformation, and thus this entire residue was omitted from the model. In contrast, Asn146, Cys147, and Ser148 could be satisfactorily modeled. The disulfide of roGFP1-iE shares the same pg$^-$t conformation as roGFP1-iR.

The 1.50 Å resolution model of reduced roGFP1-iE consists of residues 3−231, with none in the disallowed regions of the Ramachandran plot. The *R*-factor and *R*-free are 0.167 and 0.193, respectively. A $2F_o - F_c$ electron density map indicates weak density for the backbone atoms of Asn146 and side chain. The side chain of Glu147a is largely disordered and was modeled out to the Cγ. The side chains of Cys204 and Cys147 are disordered and were modeled in multiple conformations.

Comparison of Oxidized and Reduced Atomic Models. Comparisons of the oxidized and reduced states of both roGFP1-iR and roGFP1-iE reveal that, in each case, oxidation/reduction induces a dramatic "open−closed" conformational change in the segment comprised of residues 146, 147, and 147a. Interestingly, the most extreme motion of any atom

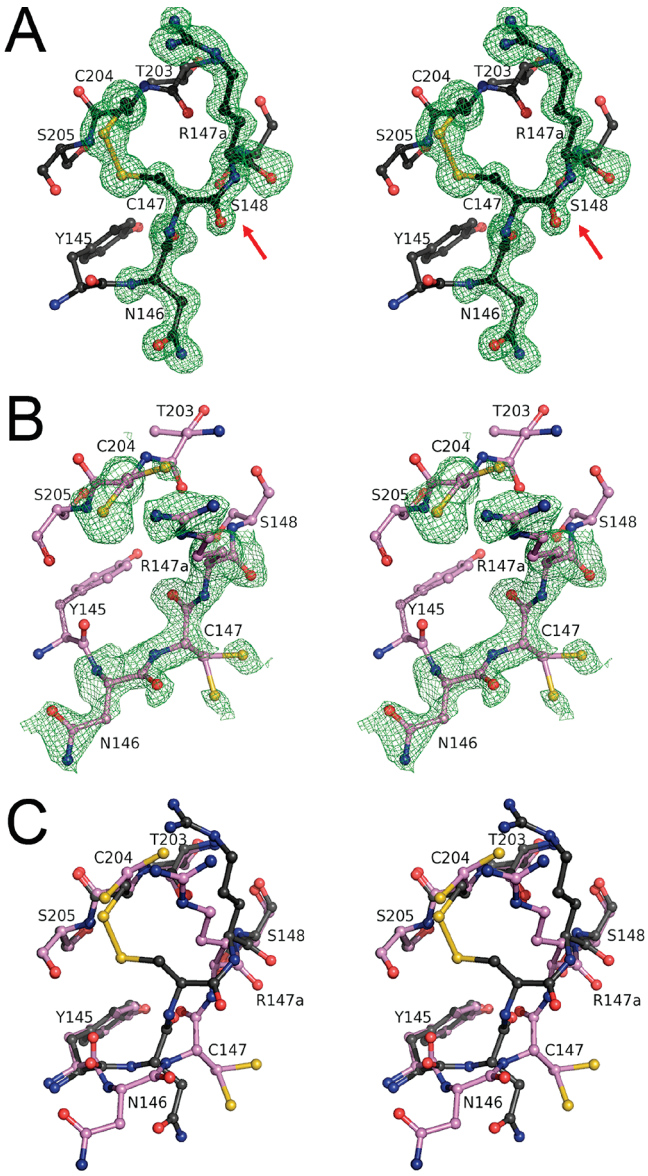

FIGURE 4: Representative electron density map and atomic models for roGFP1-iR in the oxidized and reduced states. (A) Stereo image of oxidized model superimposed on ($F_o - F_c$) omit map contoured at 3σ. Red arrow denotes non-proline cis-peptide bond. (B) Stereo image of reduced model superimposed on the ($F_o - F_c$) omit map contoured at 2.5σ. (C) Overlay of atomic models roGFP1-iR in the oxidized (black) and reduced (lavender) forms.

in the loop 146−147a is exhibited by Sγ of Cys147, which moves approximately 8 Å between the two states (see Figures 3 and 4). Furthermore, it is clear from the diffraction data for the roGFP1-iR variant that the peptide bond between residues 147 and 147a undergoes cis−trans isomerization during the transition, attaining the cis configuration in the oxidized state.

The Asn146/Cys147/X147a segment is anchored at one end by Tyr145, whose side chain is buried in the core of the protein, and at the other end by Ser148, which is pinned by backbone hydrogen bonds to the adjacent β-sheet and a hydrogen bond to the chromophore. As judged from the refined thermal parameters (*B*-factors), the open (reduced) loop conformation is characterized by a higher degree of flexibility than observed for this same segment in the closed (oxidized) state. For oxidized roGFP1-iR, the main chain *B*-factor average of Asn146/Cys147/Arg147a atoms is 15.2 Å^2, which is larger than the average of 8.9 Å^2 for the entire model (residues 7−227). In the reduced state model, the *B*-factors of this same loop are 22.6 Å^2 compared to the average of 12.9 Å^2. roGFP1-iE shows similar behavior with respect to the *B*-factors with the oxidized and reduced loops having average *B*-factors of 20.4 and 34.1 Å^2 compared to overall averages of 12.9 and 17.0 Å^2, respectively. It is possible that some of this disorder is due to X-ray induced radiation damage; however, the diffraction data were collected so as to minimize this effect. This disorder aside, the open−closed conformational change is well described by a two-state model, in which only the atoms of the segment 146−147a are seen to move.

In contrast to the segment 146−147a, the peptide containing Cys204 is essentially unresponsive to changes in the oxidation state of Cys204. The backbone is locked in place by virtue of the main chain hydrogen bonds to the neighboring β-strand (residues 221−225) and by side chains buried within the protein. However, the Cα−Cβ torsion angle of Cys204 is variable, with the Cys204 Sγ occupying at least two conformations (Figure 5).

An interesting feature of oxidized roGFP1-iR is that the hydrophobic portion of the Arg147a side chain is extended and lies adjacent to the disulfide bridge, partially shielding this group from solvent. Moreover, the Arg147a conformation is secured by a hydrogen bond between Nϵ of the guanidinium group and Oγ of Ser202. We suggest that this interaction explains the seemingly anomalous ordering of midpoint potentials within the roGFP1-iX series (see Discussion). In the reduced state, this interaction is lost, and the Arg147a side chain makes polar interactions with a neighboring molecule in the crystal. For the Glu147a variant, such a stabilizing interaction either is not possible or is energetically unfavorable, as the glutamate side chain is not ordered in either the oxidized or reduced crystals.

Comparison of roGFP1-iR and roGFP2 Disulfide Linkages. High-resolution crystal structures of the oxidized and reduced forms of roGFP2 were reported by Hanson et al. (*1*), which differs from roGFP1 by the single methyl group resulting from the substitution Ser65 → Thr. Thus roGFP2 serves as a good model for roGFP1, which is the parent for the roGFP1-iX variants described herein. In roGFP2, oxidation/reduction results in only very small changes in the positions of the Cys147 and Cys204, indicating that they are rigidly constrained by the protein fold and extensive interactions of neighboring residues. According to a statistical database on disulfide conformations compiled by Srinivasan et al. (*36*) and also by results from calculation of the disulfide energy strain (DSE) (*40*) (see Table 3), the geometry of the disulfide linkage in oxidized roGFP2 is highly strained. This was assumed to be a consequence of rigidity in the β-barrel fold of the protein. In strong contrast, large motions (up to 8 Å) of the segment 146−147a are observed upon oxidation/reduction of roGFP1-iX variants, suggesting that a great deal of flexibility is imparted by the insertion.

The flexibility derived from the insertion is further emphasized by the fact that the protein backbone of roGFP-iR accommodates the insertion between residues 147 and 148 in different ways dependent upon oxidation state (Figures 4 and 5). Two positions, Tyr145 and Ser148, pin the ends of the segment containing the insertion. Tyr145 is fixed as part of the hydrophobic core of the protein, whereas Ser148

Table 3: Comparison of Disulfide Torsion Angles[a]

	χ^{1n}	χ^{1c}	χ^{2n}	χ^{2c}	χ^{3}	Cα−Cα (Å)	Cβ−Cβ (Å)	DSE[b]
roGFP2 average	−67	−64	−100	−79	116	4.0	4.2	19.5
roGFP1-R7 average	−58	−58	−104	−78	105	4.0	4.1	15.5
rxYFP$^{147}_{202}$ average	−58	−64	−99	−83	103	3.9	4.1	14.7
roGFP1-iR	−80	180	−150	45	86	4.9	3.8	11.7
roGFP1-iE	−59	−178	−157	46	68	4.6	3.5	8.0

[a] For χ angles, n refers to N-terminal cysteine and c for C-terminal cysteine. [b] Disulfide strain energy in kJ/mol.

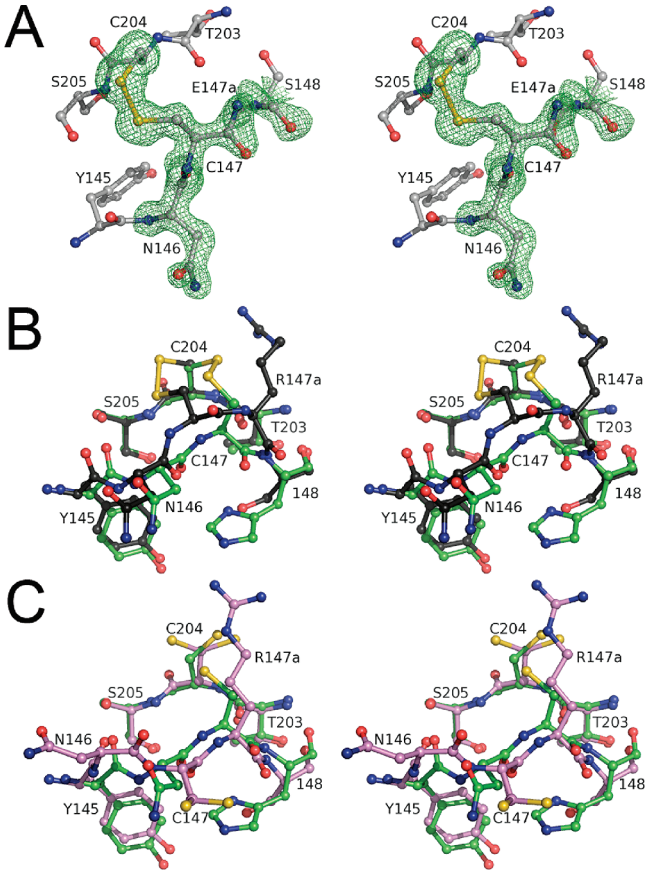

FIGURE 5: (A) Representative electron density map and overlays of atomic models for roGFP1-iE in the oxidized state. (A) Overlay of oxidized state model with ($F_o - F_c$) omit map contoured at 3σ. (B) Overlay of oxidized roGFP2 (green) and roGFP1-iR (black). (C) Overlay of reduced roGFP2 (green) and roGFP1-iR (lavender).

is oriented by hydrogen bonds in the regular β-sheet around that position. However, the intervening peptide conformation varies greatly depending upon the oxidation state of the thiol/disulfide. In the oxidized state, formation of the disulfide forces the backbone atoms of Arg147a to bulge out of the barrel. In the reduced state, Arg147a appears to be in a position similar to that of the Cys147 in roGFP1, and instead, the backbone atoms of Asn146 are bulged out. To judge from the hydrogen bond pattern, the bulge is best described as a "pseudo-bulge" in either case (*41*). Hence, the actual dislocation resulting from the insertion translocates in response to the side chain oxidation state, much as observed for insertions within the backbone of helical regions in T4 lysozyme (*42*).

For both wild-type GFP and reduced roGFP2, the *B*-factors for the strand Asn146/Ser147/His148 are comparable with those of surrounding residues, which is in contrast to reduced roGFP1-iR or roGFP1-iE, where the *B*-factors are much larger than average for this loop. This suggests that, in addition to two-state conformational flexibility (i.e., static disorder), the insertion between 147 and 148 also confers greater microscopic heterogeneity (dynamic disorder) on the backbone.

DISCUSSION

Two-state indicators that depend upon chemical equilibrium are useful for quantitative analysis over a rather narrow range, centered upon the conditions where the equilibrium constant for interconversion of the two indicator species is 1. The inevitable measurement errors introduce further restrictions on this range. In practice, roGFPs are most useful for measuring the thiol/disulfide equilibrium within ~35 mV of the indicator midpoint, corresponding to ~10−90% oxidized. For example, roGFP1 (midpoint ~−290 mV) is most useful for quantitative measurements within a range of ~−255 to −325 mV at pH 7.0 (*1*). The family shows some variation, exhibiting midpoint potentials ranging from −272 mV (roGFP2) to −299 mV (roGFP3). However, a much wider range is found within cells, with estimated values ranging from about −360 mV within mitochondria (*1, 6*) to about −180 mV within the ER (*8*). In order to have quantitative readout of thiol/disulfide redox potentials in more oxidizing environments, we require indicators with more appropriately matched midpoint potentials.

As described in the introduction, several approaches have previously led to modest destabilization of the disulfide in roGFP indicators. To achieve a more dramatic effect, we inserted single amino acid residues within the polypeptide backbone, adjacent to the reactive cysteines. We also required that the indicator response be ratiometric; in this case the response should entail a shift in equilibrium between the two chromophore forms excited at ~400 or ~475 nm. The effort produced a family of redox-sensitive fluorescent proteins termed roGFP1-iX, where the distinguishing feature of each member is the identity of X, the amino acid inserted at position 147a adjacent to Cys147.

As shown in Table 1, these variants have midpoint potentials in the range of ~−229 to ~−246 mV. Compared to the parent roGFP1, this corresponds to shifts of ~50−60 mV toward less negative midpoint potentials, indicating that the apparent equilibrium constant for disulfide formation in roGFP-iX is reduced by approximately 2 orders of magnitude. To confirm and illustrate the difference in midpoint potential, a redox titration was performed with a mixture of roGFP1 and roGFP1-iL and exhibits two distinct transitional regions (see Figure S3 in Supporting Information). All of the variants have significantly increased rates of reduction by DDT over that of the parent roGFP1; however, the rate of oxidation by cystine (CSSC) is similar for all variants.

To rationalize these results, we determined and compared the crystal structures of roGFP-iR and roGFP-iE in both the

oxidized and reduced states. In the following section, we discuss the apparent reduction in disulfide stability in terms of geometric, entropic, and electrostatic contributions.

Geometric Strain. Comparison of the 147/204 disulfide geometry (Table 3) with the statistical database compiled by Srinivasan et al. (*36*) suggests that the disulfide linkage is only slightly atypical; for example, disulfide χ^2 values of $\sim$180° are infrequently observed. We conclude that strain within the disulfide linkage is unlikely to account for its reduced thermodynamic stability, compared to the parent roGFP1. Indeed, on a geometrical basis alone, the disulfide in roGFP1-iR should be thermodynamically more stable than seen in roGFP2. However, geometric strain in the system is apparent, as illustrated by the presence of the rare and unfavorable cis-peptide bond between Cys147 and Arg147a in the oxidized form (see Figure 4). Upon reduction of the disulfide, the cis peptide bond isomerizes to the more relaxed trans form. We conclude that trans to cis peptide isomerization is required in order to form an energetically favorable disulfide linkage and that this component of the overall energetic status of the protein molecule reduces the apparent equilibrium constant for disulfide formation.

Although rare, non-proline cis−trans isomerization has been observed in other cases, suggesting that isomerization can be an important factor modulating protein activity. In concanavalin A, for example, the peptide Ala207-Asp208 undergoes trans to cis isomerization upon binding of calcium or manganese in the binuclear metal binding site. Furthermore, this isomerization reaction appears to trigger larger structural rearrangements that determine carbohydrate binding at a site distinct from the metal binding site (*43*). In both cases, the normally unfavorable trans to cis peptide bond isomerization appears to offset an even less favorable interaction at a distant site.

Entropic Effects. The solution response of roGFP-iX indicators to redox titration is accurately modeled by a theoretical curve assuming two states, open and closed, in chemical equilibrium as shown in Figure 1. However, the crystallographic results indicate that the open form of loop 146−147a has high flexibility as the *B*-factors are higher than average, consistent with conformational heterogeneity and multiple conformations (especially cysteine side chains) in the open form and thus multiple open states. In the closed state of roGFP-iR, this loop, including the side chain of Arg147a, is better ordered. This suggests that the increased number of degrees of freedom would favor the open, reduced state. The difference in flexibility of the end states is less pronounced in the roGFP-iE variant, but the trend is similar. Nevertheless, a two-state thermodynamic model is adequate to describe the transition in either case, suggesting the concept of multiple open states is not useful to explain the large reduction in thermodynamic stability of the disulfide.

From a different perspective, the large conformational change of the 147 loop, with a consequently large physical separation between the reactive cysteines in the reduced state, can be viewed as a dramatic change in effective concentration of the reacting species. This is in contrast to roGFP1, in which the cysteine side chains are held in close proximity by the protein backbone even while in the reduced state, and thus only minor rearrangements are required for disulfide formation.

Electrostatic Effects. In theory, placement of a positive charge adjacent to a disulfide should decrease its thermodynamic stability due to stabilization of the free thiolate. This has been experimentally verified by several groups (*14, 17, 44, 45*), even to the level of good quantitative agreement with nonlinear Poisson−Boltzmann theory [Cannon and Remington (*17*)]. The effect is modest, but given this good agreement between theory and experiment, counterexamples must be closely scrutinized. The family roGFP1-iX provides a case in point. Comparing the midpoint potentials of roGFP1-iR, roGFP1-iE, and roGFP1-iL (Table 1), the variant with the positively charged arginine side chain (roGFP1-iR) has the most stable disulfide. However, this apparently anomalous result can be rationalized on the basis of the crystal structure. The oxidized form reveals a specific interaction that may provide additional stabilization. In oxidized roGFP1-iR, the guanidinium moiety of Arg147a forms a hydrogen bond to Ser202 Oγ, where it is also close in space to Cys204. In the reduced state, the large loop movement in the reduced state removes the 147a side chain from the immediate vicinity of Cys204, reducing electrostatic influences at this reactive center. By comparison, the Glu147a side chain is disordered in either reduced or oxidized roGFP1-iE. We propose that the specific interaction of Arg147a with Ser202, preferentially stabilizing only the oxidized state, offsets the generalized electrostatic effects that should favor the reduced state.

We thus conclude two factors are very likely to account for the observed reduction in disulfide stability in roGFP1-iX, compared to the parent roGFP1. The first factor is geometric strain in the oxidized state (a cis peptide), while the second factor is the lowered effective concentration of the reacting species in the reduced state (due to loop opening). This argument suggests that larger insertions near the 147 position, possibly even containing the reactive cysteine, could result in further reduction of disulfide stability and, hence, in probes suitable for use in even more oxidizing environments. GFP is known to accommodate the insertion of entire proteins, such as calmodulin (*46*), in the vicinity of residue 146, so further exploration of the "insertion approach" is warranted.

Suitability of roGFP-iX Probes for Use in Vivo. Of general interest is the suitability of these probes for determination of the ambient thiol/disulfide equilibrium in relatively oxidizing environments such as the endoplasmic reticulum (ER) or the Golgi. Given that quantitative readout may be practically achieved in a range of approximately ±35 mV from the midpoint potential, the most oxidizing indicator described here (roGFP1-iL), should be useful in the range −195 to −265 mV. Assuming that the ER is −180 mV as determined from glutathione levels (*8*), it is unclear whether roGFP1-iL will be useful for quantitative measurements in that environment. Consistent with that report, the ER potential as determined by use of roGFP1 is less negative than −255 mV (*9*). However, direct determination of glutathione levels is difficult, and the literature reveals significant discrepancies in the values reported by groups using different techniques. For example, the cytosolic thiol/disulfide potential was reported by glutathione determination to be −232 mV (*8*) and by use of fluorescent redox sensors to be much more negative, at −320 mV (*5*). One possible explanation for this discrepancy is that roGFPs might

equilibrate with other reducing pools within the cell, such as NADPH via thioredoxin reductase. However, recent evidence suggests that roGFPs primarily equilibrate with the glutathione pool via glutaredoxins (*47*), as expected for protein disulfides. Thus, there is reason to suspect that the ambient potential in the ER might be more negative than indicated by measurement of glutathione and possibly within the useful range of roGFP1-iX indicators.

On a final note, the concentration of hydrogen ion factors directly into the thiol/disulfide equilibrium, and the pH range over which roGFP-iX indicators are useful is limited by additional factors. Two different effects appear to limit utility of roGFP1-iX at high and low pH. At low pH, fluorescence is quenched, while at pH $>\sim 9$, the chromophore can be titrated directly and the anionic form predominates. The quenching at low pH might be attributed to the titration of a group that indirectly determines fluorescence efficiency. However, for roGFP1-iE, the ratio of the excitation peaks is approximately constant over the pH range of 6−8 (Figure S2). The pHs of the ER and Golgi have been reported to be 7.4 and 6.2 (*48*), which is within this range. Thus, these indicators could well be useful for quantitative determination of thiol/disulfide equilibrium in such environments.

ACKNOWLEDGMENT

We thank Josef Heenan for help with the roGFP1-iX fluorescent spectral data collection and Todd O. Yeates for helpful discussions on data analysis. In addition, we thank the ALS beamline staff for maintaining and offering excellent beam time.

SUPPORTING INFORMATION AVAILABLE

Figures of data analysis and pH titrations of roGFP1-iE in oxidized and reduced states demonstrating the pH range in which the probes are useful; also a redox titration of roGFP1 and roGFP1-iL mixture to confirm the difference in redox potential. This material is available free of charge via the Internet at http://pubs.acs.org.

REFERENCES

1. Hanson, G. T., Aggeler, R., Oglesbee, D., Cannon, M., Capaldi, R. A., Tsien, R. Y., and Remington, S. J. (2004) Investigating mitochondrial redox potential with redox-sensitive green fluorescent protein indicators. *J. Biol. Chem. 279*, 13044–13053.
2. Ostergaard, H., Henriksen, A., Hansen, F. G., and Winther, J. R. (2001) Shedding light on disulfide bond formation: engineering a redox switch in green fluorescent protein. *EMBO J. 20*, 5853–5862.
3. Grynkiewicz, G., Poenie, M., and Tsien, R. Y. (1985) A new generation of Ca^{2+} indicators with greatly improved fluorescence properties. *J. Biol. Chem. 260*, 3440–3450.
4. Schafer, F. Q., and Buettner, G. R. (2001) Redox environment of the cell as viewed through the redox state of the glutathione disulfide/glutathione couple. *Free Radical Biol. Med. 30*, 1191–1212.
5. Dooley, C. T., Dore, T. M., Hanson, G. T., Jackson, W. C., Remington, S. J., and Tsien, R. Y. (2004) Imaging dynamic redox changes in mammalian cells with green fluorescent protein indicators. *J. Biol. Chem. 279*, 22284–22293.
6. Jiang, K., Schwarzer, C., Lally, E., Zhang, S. B., Ruzin, S., Machen, T., Remington, S. J., and Feldman, L. (2006) Expression and characterization of a redox-sensing green fluorescent protein (reduction-oxidation-sensitive green fluorescent protein) in Arabidopsis. *Plant Physiol. 141*, 397–403.
7. Ostergaard, H., Tachibana, C., and Winther, J. R. (2004) Monitoring disulfide bond formation in the eukaryotic cytosol. *J. Cell Biol. 166*, 337–345.
8. Hwang, C., Sinskey, A. J., and Lodish, H. F. (1992) Oxidized redox state of glutathione in the endoplasmic-reticulum. *Science 257*, 1496–1502.
9. Schwarzer, C., Illek, B., Suh, J. H., Remington, S. J., Fischer, H., and Machen, T. E. (2007) Organelle redox of CF and CFTR-corrected airway epithelia. *Free Radical Biol. Med. 43*, 300–316.
10. Austin, C. D., Wen, X. H., Gazzard, L., Nelson, C., Scheller, R. H., and Scales, S. J. (2005) Oxidizing potential of endosomes and lysosomes limits intracellular cleavage of disulfide-based antibody-drug conjugates. *Proc. Natl. Acad. Sci. U.S.A. 102*, 17987–17992.
11. Krause, G., Lundstrom, J., Barea, J. L., Delacuesta, C. P., and Holmgren, A. (1991) Mimicking the active-site of protein disulfide-isomerase by substitution of proline 34 in Escherichia-coli thioredoxin. *J. Biol. Chem. 266*, 9494–9500.
12. Wunderlich, M., and Glockshuber, R. (1993) Redox properties of protein disulfide isomerase (Dsba) from Escherichia-coli. *Protein Sci. 2*, 717–726.
13. Chivers, P. T., Prehoda, K. E., and Raines, R. T. (1997) The CXXC motif: A rheostat in the active site. *Biochemistry 36*, 4061–4066.
14. Szajewski, R. P., and Whitesides, G. M. (1980) Rate constants and equilibrium-constants for thiol-disulfide interchange reactions involving oxidized glutathione. *J. Am. Chem. Soc. 102*, 2011–2026.
15. Lees, W. J., and Whitesides, G. M. (1993) Equilibrium-constants for thiol disulfide interchange reactions—a coherent, corrected set. *J. Org. Chem. 58*, 642–647.
16. Gilbert, H. F. (1990) Molecular and cellular aspects of thiol disulfide exchange. *Adv. Enzymol. Relat. Areas Mol. Biol. 63*, 69–172.
17. Cannon, M. B., and Remington, S. J. (2006) Re-engineering redox-sensitive green fluorescent protein for improved response rate. *Protein Sci. 15*, 45–57.
18. Hansen, R. E., Ostergaard, H., and Winther, J. R. (2005) Increasing the reactivity of an artificial dithiol-disulfide pair through modification of the electrostatic milieu. *Biochemistry 44*, 5899–5906.
19. Burns, J. A., and Whitesides, G. M. (1990) Predicting the stability of cyclic disulfides by molecular modeling—Effective concentrations in thiol-disulfide interchange and the design of strongly reducing dithiols. *J. Am. Chem. Soc. 112*, 6296–6303.
20. Houk, J., and Whitesides, G. M. (1987) Structure reactivity relations for thiol disulfide interchange. *J. Am. Chem. Soc. 109*, 6825–6836.
21. Zhang, R. M., and Snyder, G. H. (1989) Dependence of formation of small disulfide loops in two-cysteine peptides on the number and types of interviening amino acids. *J. Biol. Chem. 264*, 18472–18479.
22. Pace, C. N., Grimsley, G. R., Thomson, J. A., and Barnett, B. J. (1988) Conformational stability and activity of ribonuclease-T1 with zero, one, and 2 intact disulfide bonds. *J. Biol. Chem. 263*, 11820–11825.
23. Zhang, R. M., and Snyder, G. H. (1988) Kinetics of disulfide exchange-reactions of monomer and dimer loops of cysteine valine cysteine peptides. *Biochemistry 27*, 3785–3794.
24. Woycechowsky, K. J., and Raines, R. T. (2003) The CXC motif: A functional mimic of protein disulfide isomerase. *Biochemistry 42*, 5387–5394.
25. Tsien, R. Y. (1998) The green fluorescent protein. *Annu. Rev. Biochem. 67*, 509–544.
26. Pedelacq, J. D., Cabantous, S., Tran, T., Terwilliger, T. C., and Waldo, G. S. (2006) Engineering and characterization of a superfolder green fluorescent protein. *Nat. Biotechnol. 24*, 1170–1170.
27. Siemering, K. R., Golbik, R., Sever, R., and Haseloff, J. (1996) Mutations that suppress the thermosensitivity of green fluorescent protein. *Curr. Biol. 6*, 1653–1663.
28. Patterson, G. H., Knobel, S. M., Sharif, W. D., Kain, S. R., and Piston, D. W. (1997) Use of the green fluorescent protein and its mutants in quantitative fluorescence microscopy. *Biophys. J. 73*, 2782–2790.
29. Otwinowski, Z., and Minor, W. (1997) *Processing of X-ray Diffraction Data Collected in Oscillation Mode*, pp 307−326, Academic Press, San Diego.
30. Morris, R. J., Perrakis, A., and Lamzin, V. S. (2003) ARP/wARP and automatic interpretation of protein electron density maps, in *Macromolecular Crystallography*, Part D, pp 229−244, Academic Press, San Diego.
31. Murshudov, G. N., Vagin, A. A., and Dodson, E. J. (1997) Refinement of macromolecular structures by the maximum-likelihood method. *Acta Crystallogr., Sect. D: Biol. Crystallogr. 53*, 240–255.

32. Emsley, P., and Cowtan, K. (2004) Coot: model-building tools for molecular graphics. *Acta Crystallogr., Sect. D: Biol. Crystallogr. 60*, 2126–2132.
33. Bokman, S. H., and Ward, W. W. (1981) Renaturation of Aequorea green-fluorescent protein. *Biochem. Biophys. Res. Commun. 101*, 1372–1380.
34. Ward, W. W., Prentice, H. J., Roth, A. F., Cody, C. W., and Reeves, S. C. (1982) Spectral perturbations of the Aequorea green-fluorescent protein. *Photochem. Photobiol. 35*, 803–808.
35. Ormo, M., Cubitt, A. B., Kallio, K., Gross, L. A., Tsien, R. Y., and Remington, S. J. (1996) Crystal structure of the Aequorea victoria green fluorescent protein. *Science 273*, 1392–1395.
36. Srinivasan, N., Sowdhamini, R., Ramakrishnan, C., and Balaram, P. (1990) Conformations of disulfide bridges in proteins. *Int. J. Pept. Protein Res. 36*, 147–155.
37. Jabs, A., Weiss, M. S., and Hilgenfeld, R. (1999) Non-proline cis peptide bonds in proteins. *J. Mol. Biol. 286*, 291–304.
38. Quillin, M. L., Anstrom, D. A., Shu, X. K., O'Leary, S., Kallio, K., Chudakov, D. A., and Remington, S. J. (2005) Kindling fluorescent protein from Anemonia sulcata: Dark-state structure at 1.38 angstrom resolution. *Biochemistry 44*, 5774–5787.
39. Shu, X. K., Shaner, N. C., Yarbrough, C. A., Tsien, R. Y., and Remington, S. J. (2006) Novel chromophores and buried charges control color in mFruits. *Biochemistry 45*, 9639–9647.
40. Schmidt, B., Ho, L., and Hogg, P. J. (2006) Allosteric disulfide bonds. *Biochemistry 45*, 7429–7433.
41. Richardson, J. S., Getzoff, E. D., and Richardson, D. C. (1978) The beta bulge: A common small unit of nonrepetitive protein structure. *Proc. Natl. Acad. Sci. U.S.A. 75*, 2574–2578.
42. Vetter, I. R., Baase, W. A., Heinz, D. W., Xiong, J. P., Snow, S., and Matthews, B. W. (1996) Protein structural plasticity exemplified by insertion and deletion mutants in T4 lysozyme. *Protein Sci. 5*, 2399–2415.
43. Bouckaert, J., Dewallef, Y., Poortmans, F., Wyns, L., and Loris, R. (2000) The structural features of concanavalin A governing non-proline peptide isomerization. *J. Biol. Chem. 275*, 19778–19787.
44. Huber-Wunderlich, M., and Glockshuber, R. (1998) A single dipeptide sequence modulates the redox properties of a whole enzyme family. *Folding Des. 3*, 161–171.
45. Mossner, E., Huber-Wunderlich, M., and Glockshuber, R. (1998) Characterization of Escherichia coli thioredoxin variants mimicking the active-sites of other thiol/disulfide oxidoreductases. *Protein Sci. 7*, 1233–1244.
46. Baird, G. S., Zacharias, D. A., and Tsien, R. Y. (1999) Circular permutation and receptor insertion within green fluorescent proteins. *Proc. Natl. Acad. Sci. U.S.A. 96*, 11241–11246.
47. Meyer, A. J., Brach, T., Marty, L., Kreye, S., Rouhier, N., Jacquot, J. P., and Hell, R. (2007) Redox-sensitive GFP in Arabidopsis thaliana is a quantitative biosensor for the redox potential of the cellular glutathione redox buffer. *Plant J. 52*, 973–986.
48. Wu, M. M., Grabe, M., Adams, S., Tsien, R. Y., Moore, H. P. H., and Machen, T. E. (2001) Mechanisms of pH regulation in the regulated secretory pathway. *J. Biol. Chem. 276*, 33027–33035.

BI800498G